RSC Advances

PAPER

View Article Online
View Journal | View Issue

Cite this: *RSC Adv.*, 2022, **12**, 13103

A novel strontium-based MOF: synthesis, characterization, and promising application in removal of $^{152+154}$Eu from active waste†

Mohamed A. Hamouda, [a] Sheta M. Sheta, *[b] Reda R. Sheha, [c] A. T. Kandil,[a] Omnia I. Ali[a] and Said M. El-Sheikh [d]

Removal of hazardous radioactive materials such as $^{152+154}$Eu from active waste using the batch approach has attracted attention nowadays. In this work, a novel melamine–terephthalic strontium metal–organic framework (MTSr-MOF) was prepared *via* a hydrothermal method. The MTSr-MOF was characterized by various analytical techniques such as FT-IR, ^{1}H/^{13}C-NMR, mass spectroscopy, XPS, XRD, TGA, BET, FE-SEM/EDX, TEM, and UV. The obtained data revealed that MTSr-MOF exhibited brick-like building blocks that were bridged together by the linkers, and each block had a thickness of ~120 nm. The BET surface area was 74.04 m^2 g^{-1}. MTSr-MOF was used for the removal of $^{152+154}$Eu radionuclides from active waste. Further functionalization using various modifiers, including oxalic acid, EDTA, sulfuric acid, and sodium hydroxide was carried out to improve the sorption efficiency of MTSr-MOF towards $^{152+154}$Eu radionuclides. Among them, MTSr-MOF modified with oxalic acid (MTSr-OX-MOF) demonstrated a superior removal efficiency toward $^{152+154}$Eu radionuclides when compared to MTSr-MOF or other published reports, with a removal efficiency of more than 96%. The higher sorption efficiency of the MTSr-OX-MOF indicates that it could be a promising candidate for the removal of $^{152+154}$Eu radionuclides from radioactive waste

Received 21st February 2022
Accepted 23rd April 2022

DOI: 10.1039/d2ra01159j

rsc.li/rsc-advances

Introduction

Recently, nuclear technologies have shown wide application and become one of the most important sources of energy and electricity generation in the world.[1] These applications generate considerable amounts of medium and low active wastes.[2] In addition, industries such as mining and oil production as well as research activities and medical applications produce large amounts of low active wastes.[3] These active wastes accumulate without treatment and remain hazardous for long periods.

Europium, strontium, cesium, and cobalt are the major radioactive species present in uranium fission products. The hazardous properties of these radionuclides, even at trace amounts, have caused health problems for considerable years. Thus, radioactive waste poses a significant threat to human environmental health; therefore, the radionuclides must be separated and probably managed to ensure that radiation exposure does not exceed standards and regulations. In addition, the removal of these troublesome dangerous sources and the development of an easy treatment method is vital challenges.

Many techniques have been used to remove radionuclides from active wastes such as adsorption, ion exchange, co-precipitation, liquid–liquid extraction, and chromatography.[4,5] Among these, adsorption techniques have received a wide range of interest in recent years due to their relatively low cost, simplicity, superior selectivity, and higher efficiency.[6,7] Various adsorbents are applicable for this challenge such as double layered hydroxides, layered metal sulfides, activated carbon, carbon nanotubes, clay minerals, composite materials, zeolites, and metal–organic frameworks (MOFs).[8–10] Recently, MOFs were used by many authors in this field. For example, Zhang *et al.*,[11] reported anionic-layered coordination polymer-based zirconium for the remove of Sr^{2+}. In other interested work, Zhang *et al.*,[12] reported a polyoxometalate-MOF for the capture of uranium. A radiation-resistant cationic MOFs for the removal of $^{99}TcO_4^-$ also were reported.[13,14]

MOFs are inorganic–organic hybrid materials constructed from organic linkers and metal ions (or clusters) possessing the advantages of both inorganic and organic components with unique properties.[15] Commonly, they have low density, large pore size; high thermal and chemical stability, insoluble in

[a]*Chemistry Department, Faculty of Science, Helwan University, Cairo, 11795, Egypt*
[b]*Inorganic Chemistry Department, National Research Centre, 33 El-Behouth St., Dokki, Giza, 12622, Egypt. E-mail: dr.sheta.nrc@gmail.com; Fax: +20-02-33370931; Tel: +201009697356*
[c]*Nuclear Chem. Dept., Hot Lab Center, Egyptian Atomic Energy Authority, P. O. 13759, Cairo, Egypt*
[d]*Nanomaterials and Nanotechnology Department, Central Metallurgical R & D Institute, Cairo, 11421, Egypt*

† Electronic supplementary information (ESI) available. See https://doi.org/10.1039/d2ra01159j

aqueous solutions, and extended surface area in a range from 10^3 to 10^4 m^2 g^{-1}, which enhances their suitability for removal and separation of radionuclides and toxic inorganic pollutants. MOFs have also numerous applications not only for radionuclides removal[16] but also for gas storage and separation,[17] toxic chemicals removal,[18] catalysis,[19] fuel desulfurization,[20,21] sensors/biosensors,[22–28] moisture control,[29] proton conductivity,[30] and drug delivery.[31] Furthermore, MOFs were applied for the adsorption of some radionuclides.[32–34]

Europium is considered a representative element for the trivalent actinides and its radioisotopes are listed among the hazardous species present in radioactive waste solutions. Recently, many studies were performed using different adsorbents in the separation of Eu(III) ions from aqueous active solutions for safety and environmental precautions. Sheha *et al.*[35] synthesized novel substituted hydroxyapatite nanoparticles and applied them for the removal of Eu(III) ions from aqueous active solutions. In addition, Hua *et al.*[36] fabricated a nanofibrous membrane MOF for removal of Eu(III) ions and determined a sorption capacity amounted to 191.9 mg g^{-1}. The studies on the removal of Eu(III) ions from aqueous solutions, using MOFs as sorbents, were slightly observed.

Herein, a novel melamine–terephthalic strontium metal–organic framework (MTSr-MOF), was synthesized *via* a hydrothermal process. The prepared MOF was fully characterized and applied for the removal of Eu(III) ions from an aqueous active solution. Moreover, the surface of the prepared MOF was functionalized using different modifiers to enhance its affinity towards Eu(III) ions.

Results and discussion

MTSr-MOF-NPs characterization

Characterization of the prepared MOF. The CHN analysis of synthesized MTSr-MOF as represented in (Fig. 1) compared with the theoretically calculated data is given in (Table S1†). The analytical data for MTSr-MOF revealed that the product has MT_2Sr_2. 2DMF as a molar mass ratio with a formula $C_{25}H_{26}Cl_2N_8O_8Sr_2$, (812.67 g mol^{-1}). The theoretically calculated CHN masses were C, 36.95; H, 3.22; and N, 13.79, while the experimentally determined ones were C, 37.61; H, 2.94; and N, 13.69, respectively. The data clarify that the theoretically calculated values were consistent with the experimentally determined ones, elucidating the successful preparation of MTSr-MOF with a yield of 87.11% and m. p. over 300 °C. Using the collected micro/analytical data, the explication and optimization of the MOF proposed structure were examined as follows:

SEM/EDX and TEM. The SEM images reveal that the particles of MTSr-MOF appeared as 2D sheets of brick-like building blocks, (Fig. 2a–h). Each block had an aspect ratio of 0.5 with a height ranging from 100–150 nm, (Fig. 2a and b). It was noticed that the surface of each block had spherical nanoparticles whose size ranged from 17–30 nm, (Fig. 2c and d). Additionally, other spherical particles that appeared on the surface of blocks had sizes ranging from 115–200 nm, (Fig. 2e and f). An overview, on a large scale, of the blocks, is presented in (Fig. 2g and h). The mapping data analysis of MTSr-MOF, performed by EDX, showed the presence of "oxygen, nitrogen, carbon, chlorine, and strontium" as block construction elements, (Fig. 3a–g) and (Table S1†). The live mapping of EDX is given in (Fig. 3a) while (Fig. 3b) shows the coloured elements mapping through a single point analysis and that for each element individually is displayed in (Fig. 3c–g). Along with the cross-section exhibited by EDX mapping, the data revealed an

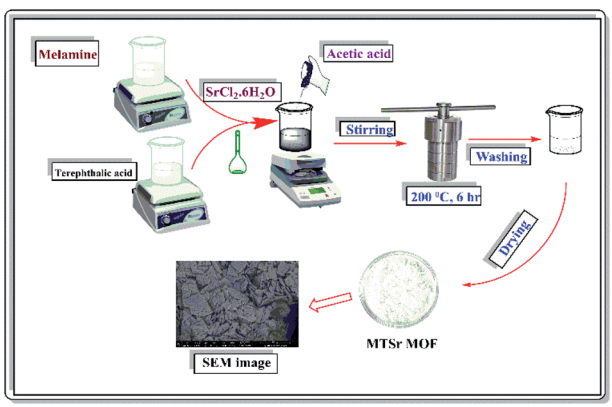

Fig. 1 The synthetic scheme followed in MTSr-MOF preparation.

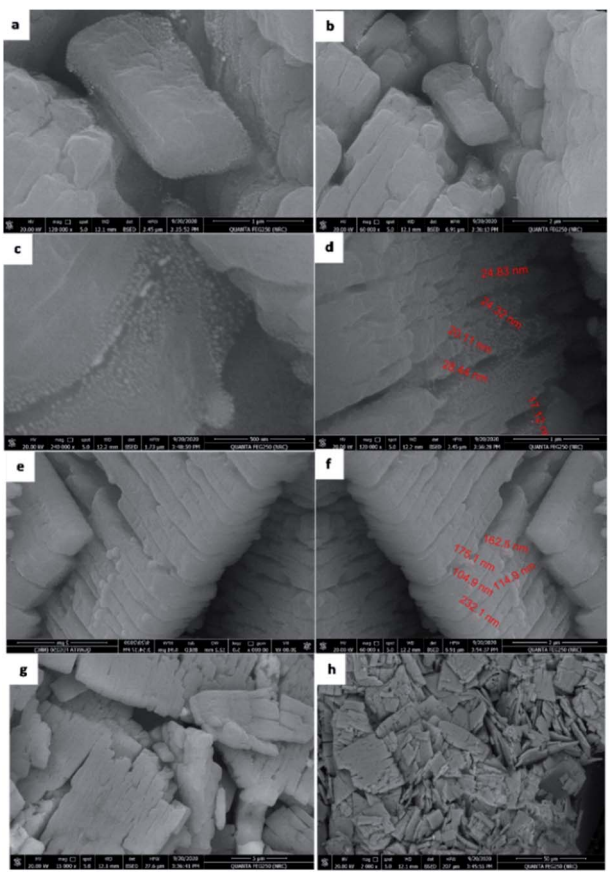

Fig. 2 The field-emission scanning electron microscopy of MTSr-MOF at different magnifications.

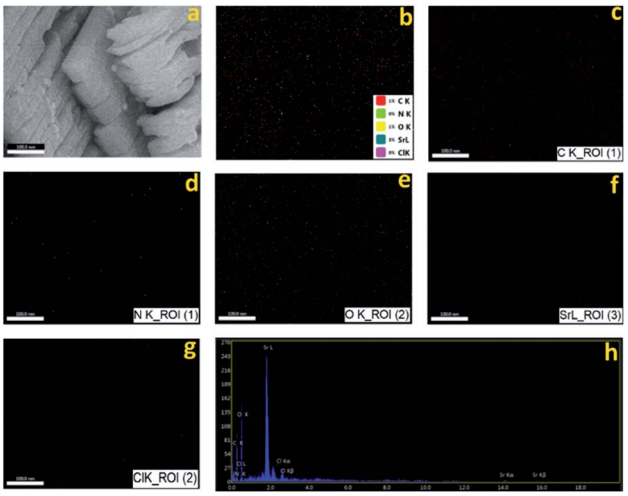

Fig. 3 The energy-dispersive X-ray analysis with a single point EDX mapping analysis of MTSr-MOF: (a) the image of live mapping of EDX; (b) the coloured elements block mapping through a single point analysis; (c–g) individual elemental map colour for carbon, nitrogen, oxygen, strontium, and chlorine, respectively; (h) the EDX mapping of the block elements.

outstanding distribution of block elements, as shown in, (Fig. 3h). The revealed data confirmed the successful formation of MTSr-MOF. Moreover, the percentage of elemental mapping was in good conformity with the elemental percentage that was calculated theoretically, (Table S1†). The theoretical values were: C, 36.95; Cl, 8.72; N, 13.79; O, 15.75; Sr, 21.56; while the experimental values were: C, 36.66; Cl, 8.35; N, 12.87; O, 21.19; and Sr, 20.93, respectively. TEM images show the porosity of the MTSr-MOF and the spherical nanoparticles that appeared more clearly on the surface of each block with a diameter range of 15–30 nm, (Fig. 4a and b). These results are in good agreement with those obtained from FE-SEM data, (Fig. 4c).

UV analysis. The absorption spectrum of the prepared MTSr-MOF is shown in (Fig. S1†). The spectrum revealed absorption bands only in the UV region. The MTSr-MOF has four bands that appeared at 233, 276, 315, and 345 nm. The bands at 233 and 276 nm in MTSr-MOF may be attributed to the ligands, melamine and terephthalic acid, with a bathochromic shift of the original λ_{max} of melamine and terephthalic acid at 210 and 240–250 nm, respectively.[37] These results are clear evidence of the interaction between the starting ligands.

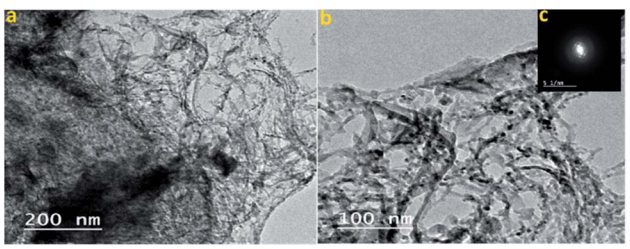

Fig. 4 The transmission electron microscopy image (TEM) and SAED images of MTSr-MOF.

FT-IR spectra. The prepared MTSr-IR spectrum is displayed in (Fig. S2†). The peaks recorded at 3396 and 3470 cm^{-1} could be attributable to the amide linkage's N–H stretching frequency, which proved the formation of an amide linkage between the carboxylic and amine groups of terephthalic and melamine ligands.[38] The peak observed at 1641 cm^{-1} may be attributed to the presence of stretching C=O that was broadened with multiple splitting. This may be due to the inclusion of C=O through amide linkage, which caused a shift to a lower frequency rather than the C=O peak in terephthalic acid at 1690 cm^{-1}.[39] The three peaks revealed at 569, 518, and 452 cm^{-1} were characteristic bands of strontium bonding (Sr–O), which is clear evidence for the existence of Sr–O coordination bonds in MTSr-MOF. Besides, the peak of N–H sp^2 of melamine at 3418 cm^{-1} disappeared, while two new peaks were observed at 3325 and 3126 cm^{-1} and could be ascribed to N–H sp^2 and N–H sp^3 of melamine.[38]

^{1}H and ^{13}C NMR spectra. The experimental ^{1}H NMR spectrum of MTSr-MOF is given in (Fig. S3†). The figure shows eleven signals at δ 1.9, 2.5, 2.8, 6.75, 7.81, 7.83, 7.9, 8.03, 8.09, 8.208, and 8.22 ppm. The signal at 2.5 and the weak intense signal at 2.8 ppm were attributed to the solvent (DMSO) and the presence of water molecules, respectively.[40] The signal observed at 6.75 ppm was attributed to $-NH_2$ and the signals at 7.81 and 7.83 ppm were attributed to amide protons.[41] The broad signal detected at 7.12 ppm was attributed to the acidic $-NH_2$ protons.[42] The broadening may be due to the exchangeable ability of these acidic protons, which resulted in no coupling with their neighbour protons. While the signals at 7.9, 8.03, 8.20, and 8.22 ppm were attributed to the aromatic protons.[40] The experimental ^{13}C-NMR full spectrum of MTSr-MOF is depicted in (Fig. S4†). The spectrum includes five signals at δ 39.5, 130.2, 136, 164.3, and 169.15 ppm. The signal that appeared at 39.5 ppm was attributed to the solvent signals of DMSO. The aromatic carbons showed signals at 130.2 and 136 ppm.[43] The signal at 164.3 ppm was attributed to the amide carbon. Finally, the signal at 169.1 ppm was referred to as the carbon of the carboxylic group O=C–O.[44]

Mass spectrum. Fig. S5 and S6† represent the mass spectrum and the proposed fragmentation of MTSr-MOF, respectively. The molecular ion peak of MTSr-MOF was observed at 830 m/z, which corresponded to the proposed structure. The base peak for MTSr-MOF appeared at 126 m/z. The subsequent theoretical fragmentation appears slightly consistent with the molecular weight of the proposed structure.

Thermal analysis. The thermal stability of MTSr-MOF was tested under nitrogen gas for 1000 °C/10 °C per minute (Fig. S7†). The thermogram indicates that the decomposition of MTSr-MOF went through two stages. The first stage exhibited a weight loss amounted to ~18.12% with a rising temperature up to ~250 °C. This loss could be attributed to the evaporation loss of solvent molecules. With further increase in temperature up to ~350 °C (2nd stage), the thermogram showed a loss in the sample weight amounted to ~70.9%, this loss was followed by an endothermic peak at around 300 °C, it might be ascribed to internal water molecule evaporation, collapsing of linker

molecules, and formation of a completely dried metal–organic framework with a crystalline structure. At higher temperatures, the analysed MOF showed considerable thermal stability up to ~1000 °C with a slight loss. The remaining residue that amounted to ~20.9%, determined the metallic Sr-content in the MOF sample. This result is consistent with the data obtained from EDX analysis.

XPS analysis. The MTSr-MOF XPS-survey spectrum is illustrated in (Fig. 5a). In the spectrum, O 1s, C 1s, N 1s, and Sr 3d were all recognized. The high-resolution fitting of MTSr-MOF O 1s is shown in (Fig. 5b). The peaks at 530.30, 531.49, and 532.80 eV were ascribed to the presence of C═O, Sr–O bond, and C–O, respectively.[45] The presence of Sr–O peaks illustrated the formation of coordination bonds between the terephthalic acid's oxygen and Sr. The XPS fitting for N 1s of prepared MTSr-MOF is presented in (Fig. 5c). The spectrum shows two characteristic peaks at a binding energy of 398.52 and 399.38 eV. The peak detected at 398.52 eV was assigned to the amide group (N–C═O) that proved the formation of amide linkage between melamine and terephthalic acid ligands.[46,47] The other peak observed at 399.38 eV could be attributed to N═C bonds of the heterocyclic melamine. (Fig. 5d) shows the high-resolution XPS for C 1s of the MTSr-MOF sample. The figure shows three peaks were observed at 284.47, 284.66, and 288.10 eV which were assigned to C═C, C═N, and O═C–N, respectively. The Sr 3d, de-convolution of MTSr-MOF showed peaks at 127.89, 129.72, 133.39, and 136.29 eV, which were related to Sr 3d5/2 as well as Sr 3d3/2 (Fig. 5e).[48]

XRD analysis. Fig. 5f demonstrates the XRD spectrum of the synthesized MTSr-MOF. The crystallinity was calculated using the crystallinity index (about 50%) and the data confirmed that the prepared MOF show a good crystalline quality. The diffractogram shows two peaks at 26.35° and 39.5° that correspond to the two characteristic peaks of melamine with a little shift was observed in the position of the former peaks and disappearance of the other peaks, and this confirmed that melamine had participated in the synthesis of the obtained MOF.[38] The peaks at 2θ; 17.21°, 25.07°, and 29.57° that represent the terephthalic acid peaks showed a small deviation from the characteristic peaks of pure terephthalic acid.[49] Further three peaks were detected at 13.62°, 27.67°, and 31.76° which could be considered as characteristic peaks of strontium chloride hexahydrate with a small shift from its ideal peaks' positions. The presence of new peaks at 2θ; 12.6°, 18.40°, 28.62°, 37.40°, and 40.82° was clear evidence for the formation of the new phase of prepared MOF.

BET analysis. The nitrogen adsorption/desorption isotherm of MTSr-MOF is shown in (Fig. 6a). The isotherm corresponds to type IV, actually, the main pore size is located about 1.7 nm which is a micropores zeolitic structure with a minor mesopores intermediate surfaces.[50,51] The MTSr-MOF's BET surface area was determined and observed to be 74.07 m^2 g^{-1}. Further, MTSr-MOF's surface area was calculated using several methods such and the obtained values are summarized in (Table S2†). The results of pore size distribution and pore volume of MTSr-MOF are represented in (Tables S3 and S4†). The MTSr-MOF's surface area was determined using different methods that obtained varied values which represented zeolitic structure.

Based on the obtained microanalytical data, the optimization of the MTSr-MOF 3D-structure and total charge density of

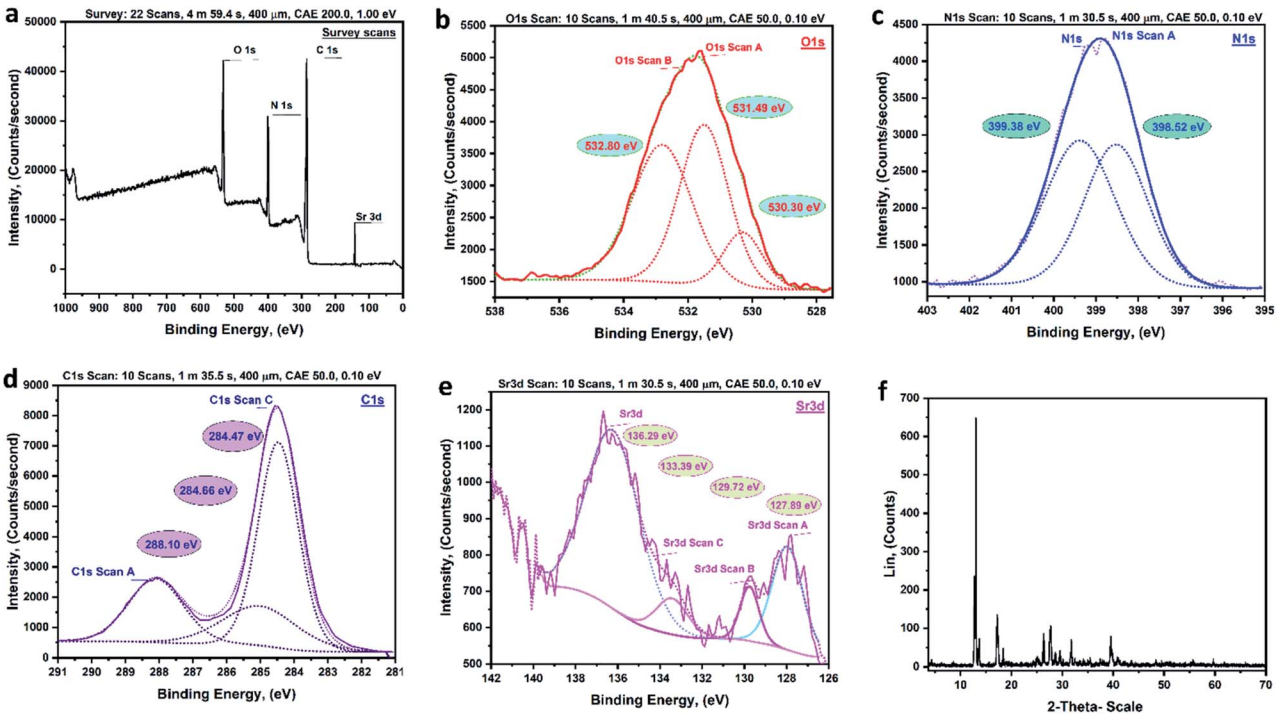

Fig. 5 The X-ray photoelectron spectroscopic analysis (XPS) and X-ray diffraction (XRD) of MTSr-MOF [(a) survey scan, (b) O 1s, (c) N 1s, (d) C 1s, (e) Sr 3d, and (f) XRD pattern].

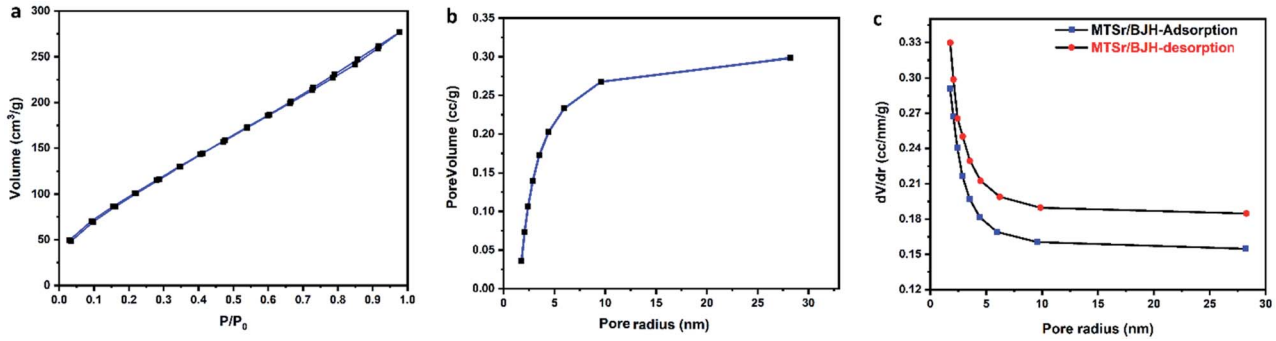

Fig. 6 The BET surface area analysis of MTSr-MOF: (a) N_2 adsorption/desorption isotherm, (b) the BJH pore volume, and (c) changes in pore size distribution in relation to pore radius.

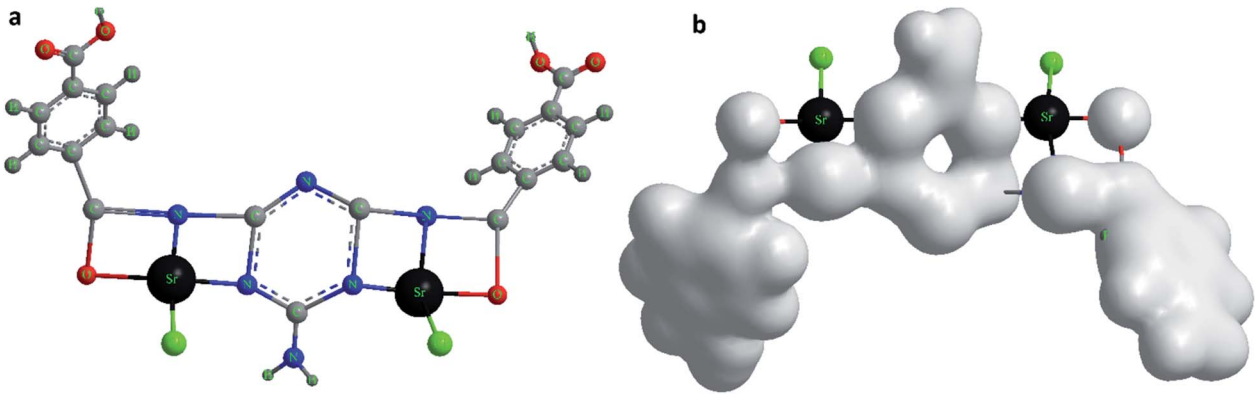

Fig. 7 (a) The 3D structural representation of MTSr-MOF monomeric unit, and (b) total charge density of advanced molecular surface representation of MTSr-MOF monomeric unit.

advanced molecular surface may be suggested as illustrated in (Fig. 7a and b).

Eu(III) sorption. The prepared MOF and its modified precursors were applied in the removal of $^{152+154}$Eu radionuclides from active aqueous solution and data revealed are presented in (Fig. 8). The plots show that MTSr-MOF exhibited a low affinity towards Eu species. Where only 13.59% was eliminated from the aqueous active solution upon achieving equilibrium. Similarly, the modified MOF samples slightly removed ions of Eu(III) from their aqueous solutions except for oxalic-modified precursor. The uptake percent of Eu ions attained the values 13.59, 12.22, 12.78, and 10.42% for sorption onto MTSr-MOF, MTSr-EDTA, MTSr-SO_4, and MTSr-NaOH, respectively. In contrast, the MOF sample modified with oxalic acid exhibited a superior affinity towards Eu isotopes, where more than 96% of Eu isotopes were retained within this sorbent after equilibrium.

Table 1, shows a comparison of the adsorption capacities of the $^{152+154}$Eu radionuclides with different materials from the available literature. In this work, the adsorption capacity value of the prepared MTSr-OX-MOF is higher than the results published before. This indicates that the MTSr-OX-MOF is seen as a promising material for removing $^{152+154}$Eu radionuclides from radioactive waste. Full characterization and statistical evaluation of the new modified MTSr-MOF will be investigated in near future work as well as more studies in this hot point could be targeted in the future. Moreover, from the table data Zheng *et al.*,[52] was used titanate nano-rings for removal of Eu ions with a capacity of about 98% but the study investigated the

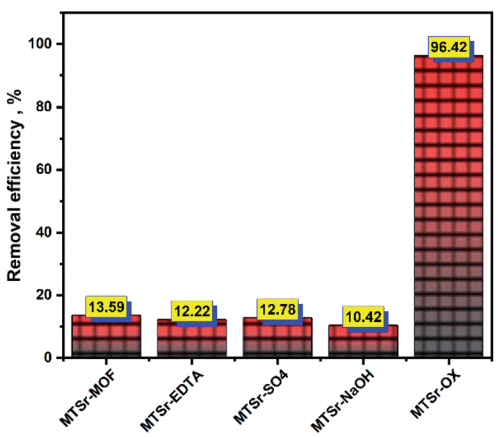

Fig. 8 The removal of $^{152+154}$Eu radionuclides from active solutions using different modified MOFs ($C_i = 20$ mg L^{-1}, pH = 3.5, $\frac{v}{m} = 10$, temp = 25 ± 1 °C).

Table 1 Removal efficiency comparison of MTSr-MOF for Eu(III) with other different materials

Adsorbents	Removal efficiency %	References
Perlite	17	53
Zirconium MOF M1	36	54
Modified silica nanoparticles	85	55
MoS_2/carbon nanocomposite	86.5	56
Modified perlite	97	53
Titanate nano-rings	98.1	52
MTSr-MOF	13.6	This work
MTSr-EDTA-MOF	12.22	This work
MTSr-SO_4-MOF	12.78	This work
MTSr-NaOH-MOF	10.42	This work
MTSr-OX-MOF	96.42	This work

optimum pH for adsorption observed at 5–6 and this no *t* regard an absolute adsorption but it's a mixture between adsorption and precipitation due to europium presented in aqueous solution mainly as Eu^{3+} species up to pH 4.

Experimental

Materials

All chemicals and reagents used for the synthesis of MTSr-MOF and modified MTSr-MOFs were of analytical grade and were used without further purification. Melamine was supplied from Alfa-Aesar (Germany) and strontium chloride hexahydrate from NICE (India). Terephthalic acid, ethanol, and glacial acetic acid were supplied from Sigma-Aldrich (Germany). ARE-RR2 reactor in Egypt manufactured $^{152+154}$Eu radioisotopes by neutron irradiating a stable target of this element. The specific weight of europium oxide was placed in a thin sheet of high purity aluminium and irradiated for a specific amount of time within the reactor. The sample was irradiated, then allowed to cool before being dissolved in a little amount of strong hydrochloric acid. The solution was heated to dryness after full dissolution and then redissolved in a specific volume of bi-distilled water.

Instruments

MTSr-MOF was characterized using various techniques. Costech's ECS-4010 analyzer was used to do elemental analysis (C, H, and N). A field emission-scanning electron microscope (FE-SEM) of type (JEOL JSM-6510LV) from Japan was used to evaluate the surface morphology of the fabricated MOF. The elemental mapping was examined using spatially resolved energy-dispersive X-ray spectroscopy. A [JEOL JSM-6510LV QSEM Advanced electron microscope with a LAB-6 cathode at 520 keV] was used for the analysis. A high-resolution transmission electron microscope (HR-TEM) with an acceleration voltage of up to 200 keV [TEM, JEOL-JEM-2100, Japan] was used to study the morphology of the produced phase. UV-visible absorption spectroscopy was used to record the absorption spectrum of the synthesized MOF using a UV/VIS-JASCO V-770 spectrophotometer. The organic groups of the synthesized MOF were examined using a Fourier transform infrared FTIR-JASCO 3600-spectrometer in the range (400–4000 cm^{-1}) and KBr tablets at room temperature. In DMSO-d6, ^{1}H-NMR and ^{13}C-NMR spectra were analyzed using a JEOL Gemini-300 MHz NMR spectrometer (model ECA 500 II). Thermo Scientific's IQS Single Quadrupole MS was used to record the mass spectrum of the MTSr-MOF sample. Thermogravimetric analysis (TGA) was accomplished on the constructed MOF using an SDTQ600 analyser at a rate of 10 °C min^{-1} under argon to evaluate its thermostability. X-ray photoelectron spectroscopy (XPS) measurements investigated the elements that existed within the synthesized MOF or cover its surface as well as their chemical states. The analysis was carried out using [Thermo Scientific™ K-Alpha™ XPS spectrometer, equipped with Al-Kα microfocused monochromator within an energy range up to 4 keV]. To characterize the crystalline phase and relative crystalline nature of as-prepared MOF, X-ray diffraction (XRD) pattern was performed using a D8 advance X-ray diffractometer [Bruker AXS D8, Germany] equipped with Cu-K radiation (= 0.154056 nm). With a 0.04° step and a scanning speed of 0.4 s, the sample was detected in the range of 2 from 4 to 70°. For the measurement of the effective surface area of the produced MOF sample, Brunauer–Emmett–Teller (BET) was utilized as an analysis technique. A single channel analyser of the Nucleus-500 type linked to an NJ scintillation detector was used to measure the activity of $^{152+154}$Eu isotopes.

Procedure

MTSr-MOF synthesis. A hydrothermal method was adopted for the synthesis of MTSr-MOF using melamine (M), terephthalic acid (T), and strontium chloride hexahydrate with molar ratios of 1 : 2 : 2, respectively, as represented in (Fig. 1). 0.316 g (1.0 mmol) of melamine was completely dissolved in 15.0 mL distilled water, then 5.0 mL of DMF was added to the melamine solution. 1.066 g (2.0 mmol) of $SrCl_2 \cdot 6H_2O$ was dissolved in a small amount of water and added to melamine solution with stirring for 30 min and referred to as (solution A). After that, 0.668 g (2.0 mmol) of terephthalic acid was dissolved in 10 mL DMF and added dropwise solution-A with continuous stirring, then a white colour immediately appeared, and the mixture was noted as (solution B). One mL of glacial acetic acid was added to (solution B) as a modulator and the solution was stirred for 30 min. The solution-B was placed in a stainless autoclave with Teflon lining and heated for 8 hours at 200 °C. Allow to cool to room temperature, a fine white powder of MTSr-MOF was obtained, filtered, washed (with distilled water and ethanol), and vacuum dried at 50 °C for 24 h.

Functionalization and modification of MTSr-MOF

The obtained MTSr-MOF was soaked in a 0.05 mol L^{-1} solution of various modifiers, including EDTA, H_2SO_4, NaOH, and oxalic acid for 24 hours. The obtained MTSr-EDTA, MTSr-H_2SO_4, MTSr-NaOH, and MTSr-OX MOFs were filtered, rinsed (with deionized and ethanol), and then vacuum-dried at 60 °C for 24 h.

Primary sorption studies

The batch approach was used to investigate the plucking out of the efficiency of unmodified and modified MOFs against the radionuclides $^{152+154}$Eu. The sorption of europium onto the surface of the synthesized MOFs was investigated by equilibrating MOFs samples with europium solutions having 20 mg L^{-1} initial concentration and spiked with $^{152+154}$Eu traces. 0.01 g MOF samples were merged with a certain volume of Eu(III) solution and shacked overnight in a thermostatic shaker at 25 ± 1 °C. After equilibrium, to assess the activity of $^{152+154}$Eu, the supernatant was collected and subjected to a radiometric experiment. The removal efficiency percentage of Eu(III) (E%) was obtained from (eqn (1)):

$$E\% = \frac{A_i - A_f}{A_i} \times 100 \quad (1)$$

where: A_i and A_f are the initial and final activities of the europium active solution after and before the sorption process.

Conclusions

This work presents a novel strontium-based metal–organic framework (MTSr-MOF) which could be considered as a bright prospect candidate to the successful removal of Eu(III) radioisotopes from active solutions. The prepared MTSr-MOF was well-characterized using different analytical and microanalytical tools. The results revealed that MTSr-MOF exhibited as brick-like building blocks with a thickness of each block of about 120 nm. The MTSr-MOF showed a lower removal percentage of about 13.59%. Therefore, the MTSr-MOF was modified using different modifiers, and the results revealed that MTSr-MOF modified with oxalic acid exhibited a superior removal efficiency for $^{152+154}$Eu radionuclides of about 96.42% more than the other modified MOFs. That could be a promising candidate for the removal of $^{152+154}$Eu radionuclides from radioactive waste in the future.

Conflicts of interest

There are no conflicts to declare.

Acknowledgements

A part of this work was supported by the financial support of the Science and Technology Development Fund (STDF) Foundation of the project no. (37068).

Notes and references

1 S. Bilgen, *Renewable Sustainable Energy Rev.*, 2014, **38**, 890–902.
2 C. Cabaud, Y. Barré, L. De Windt, S. Gill, E. Dooryhée, M. P. Moloney, N. Massoni and A. Grandjean, *Adsorption*, 2019, **25**, 765–771.
3 Z. H. Saidin, *21st EGU Gen. Assem. EGU, Proc. Conf. held 7–12 April*, Vienna, Austria, 2019.
4 M. F. Attallah, S. E. Rizk and S. A. Shady, *Nucl. Sci. Tech.*, 2018, **29**, 84.
5 R. R. Sheha, *J. Colloid Interface Sci.*, 2012, **388**, 21–30.
6 W. Lin, Z. Zhao, F. Yang, Z. Liu, F. Tan, M. Xie, Y. Ma and L. Meng, *Miner. Eng.*, 2021, **164**, 106831.
7 R. T. Yang, *Adsorbents: Fundamentals and Applications*, John Wiley & Sons, 2003.
8 J. Li, X. Wang, G. Zhao, C. Chen, Z. Chai, A. Alsaedi, T. Hayat and X. Wang, *Chem. Soc. Rev.*, 2018, **47**, 2322–2356.
9 H. S. Hassan, M. I. A. A. Maksoud and L. A. Attia, *J. Mater. Sci.: Mater. Electron.*, 2020, **31**, 1616–1633.
10 R. R. Sheha and S. H. El-Khouly, *Chem. Eng. Res. Des.*, 2013, **91**, 942–954.
11 J. Zhang, L. Chen, X. Dai, L. Zhu, C. Xiao, L. Xu, Z. Zhang, E. V. Alekseev, Y. Wang, C. Zhang, H. Zhang, Y. Wang, J. Diwu, Z. Chai and S. Wang, *Chem*, 2019, **5**, 977–994.
12 H. Zhang, W. Liu, A. Li, D. Zhang, X. Li, F. Zhai, L. Chen, L. Chen, Y. Wang and S. Wang, *Angew. Chem., Int. Ed.*, 2019, **58**, 16110–16114.
13 L. Zhu, D. Sheng, C. Xu, X. Dai, M. A. Silver, J. Li, P. Li, Y. Wang, Y. Wang, L. Chen, C. Xiao, J. Chen, R. Zhou, C. Zhang, O. K. Farha, Z. Chai, T. E. Albrecht-Schmitt and S. Wang, *J. Am. Chem. Soc.*, 2017, **139**, 14873–14876.
14 D. Sheng, L. Zhu, X. Dai, C. Xu, P. Li, C. I. Pearce, C. Xiao, J. Chen, R. Zhou, T. Duan, O. K. Farha, Z. Chai and S. Wang, *Angew. Chem.*, 2019, **131**, 5022–5026.
15 M. B. Majewski, H. Noh, T. Islamoglu and O. K. Farha, *J. Mater. Chem. A*, 2018, **6**, 7338–7350.
16 T. Zheng, Z. Yang, D. Gui, Z. Liu, X. Wang, X. Dai, S. Liu, L. Zhang, Y. Gao, L. Chen, D. Sheng, Y. Wang, J. DIwu, J. Wang, R. Zhou, Z. Chai, T. E. Albrecht-Schmitt and S. Wang, *Nat. Commun.*, 2017, **8**, 1–11.
17 W. G. Cui, T. L. Hu and X. H. Bu, *Adv. Mater.*, 2020, **32**, 1–24.
18 H. C. Woo and S. H. Jhung, *Chem. Eng. J.*, 2021, **425**, 130598.
19 N. Antil, A. Kumar, N. Akhtar, R. Newar, W. Begum, A. Dwivedi and K. Manna, *ACS Catal.*, 2021, **11**, 3943–3957.
20 L. Guo, J. Du, C. Li, G. He and Y. Xiao, *Fuel*, 2021, **300**, 120955.
21 M. Huang, G. Chang, Y. Su, H. Xing, Z. Zhang, Y. Yang, Q. Ren, Z. Bao and B. Chen, *Chem. Commun.*, 2015, **51**, 12205–12207.
22 S. M. Sheta, S. M. El, S. Mohkles, M. A. Elzaher and A. R. Wassel, *Appl. Organomet. Chem.*, 2019, **33**, e4777.
23 A. S. Basaleh and S. M. Sheta, *Anal. Bioanal. Chem.*, 2020, **412**, 3153–3165.
24 S. M. Sheta, S. M. El-sheikh and M. M. Abd-elzaher, *Anal. Bioanal. Chem.*, 2019, **411**, 1339–1349.
25 S. M. Sheta, S. M. El-sheikh, D. I. Osman, A. M. Salem, O. I. Ali, F. A. Harraz, W. G. Shousha, M. A. Shoeib, S. M. Shawky and D. D. Dionysiou, *Dalton Trans.*, 2020, **49**, 8918–8926.
26 S. M. El-sheikh, D. I. Osman, O. I. Ali, W. Gh, M. A. Shoeib, S. M. Shawky and S. M. Sheta, *Appl. Surf. Sci.*, 2021, **562**, 150202.
27 S. M. Sheta, S. M. El-Sheikh and M. M. Abd-Elzaher, *Appl. Organomet. Chem.*, 2019, **33**, e5069.

28 M. Alhaddad and S. M. Sheta, *ACS Omega*, 2020, **5**, 28296–28304.
29 R. G. Abdulhalim, P. M. Bhatt, Y. Belmabkhout, A. Shkurenko, K. Adil, L. J. Barbour and M. Eddaoudi, *J. Am. Chem. Soc.*, 2017, **139**, 10715–10722.
30 M. J. Wei, B. Li, H. Y. Li, L. Zhang, Y. T. Luo, H. Y. Zang, W. Wang, D. H. Fan, K. Z. Shao and Z. M. Su, *J. Solid State Chem.*, 2020, **290**, 121550.
31 J. W. M. Osterrieth and D. Fairen-Jimenez, *Biotechnol. J.*, 2021, **16**, 2000005.
32 C. Xiao and S. Wang, *11 – Radionuclide Sequestration by Metal–Organic Frameworks, Metal–Organic Frameworks (MOFs) for Environmental Applications*, ed. S. K. Ghosh, Elsevier, 2019, pp. 355–382.
33 L. Li, W. Ma, S. Shen, H. Huang, Y. Bai and H. Liu, *ACS Appl. Mater. Interfaces*, 2016, **8**, 31032–31041.
34 S. Naeimi and H. Faghihian, *Sep. Purif. Technol.*, 2017, **175**, 255–265.
35 R. R. Sheha, S. I. Moussa, M. A. Attia, S. A. Sadeek and H. H. Someda, *J. Environ. Chem. Eng.*, 2016, **4**, 4808–4816.
36 W. Hua, T. Zhang, M. Wang, Y. Zhu and X. Wang, *Chem. Eng. J.*, 2019, **370**, 729–741.
37 J. Tan, R. Li and Z. T. Jiang, *Food Anal. Methods*, 2012, **5**, 1062–1069.
38 M. S. L. Rosa, T. Knoerzer, F. C. Figueiredo and J. R. dos Santos, *Polimeros*, 2020, **30**, e2020004.
39 S. A. Ravichandran, V. P. Rajan, P. V. Aravind, A. Seenivasan, D. G. Prakash and K. Ramakrishnan, *Macromol. Symp.*, 2016, **361**, 30–33.
40 M. Heidari, A. Sedrpoushan and F. Mohannazadeh, *Org. Process Res. Dev.*, 2017, **21**, 641–647.
41 R. J. Abraham, L. Griffiths and M. Perez, *Magn. Reson. Chem.*, 2014, **52**, 395–408.
42 S. M. Sheta, S. M. El-Sheikh, M. M. Abd-Elzaher, M. L. Ghanemc and S. R. Salem, *RSC Adv.*, 2019, **9**, 20463–20471.
43 S. Bennabi and M. Belbachir, *J. Inorg. Organomet. Polym. Mater.*, 2017, **27**, 1787–1799.
44 M. G. Mohamed, C. H. Hsiao, F. Luo, L. Dai and S. W. Kuo, *RSC Adv.*, 2015, **5**, 45201–45212.
45 J. C. Dupin, D. Gonbeau, P. Vinatier and A. Levasseur, *Phys. Chem. Chem. Phys.*, 2000, **2**, 1319–1324.
46 H. Awada, D. Monplaisir and C. Daneault, *BioResources*, 2012, **7**, 2090–2104.
47 P. K. Rastogi, K. R. Sahoo, P. Thakur, R. Sharma, S. Bawari, R. Podila and T. N. Narayanan, *Phys. Chem. Chem. Phys.*, 2019, **21**, 3942–3953.
48 D. J. Kim and W. K. Jo, *Appl. Catal., B*, 2019, **242**, 171–177.
49 X. Dyosiba, J. Ren, N. M. Musyoka, H. W. Langmi, M. Mathe and M. S. Onyango, *Ind. Eng. Chem. Res.*, 2019, **58**, 17010–17016.
50 I. Nongwe, V. Ravat, R. Meijboom and N. J. Coville, *Appl. Catal., A*, 2016, **517**, 30–38.
51 K. V. Kumar, S. Gadipelli, B. Wood, K. A. Ramisetty, A. A. Stewart, C. A. Howard, D. J. L. Brett and F. Rodriguez-Reinoso, *J. Mater. Chem. A*, 2019, **7**, 10104–10137.
52 M. Zheng, H. Ji, J. Duan, C. Dang, X. Chen and W. Liu, *Environ. Sci. Ecotechnology*, 2020, **2**, 100031.
53 I. M. Ahmed, L. A. Attia and M. F. Attallah, *Radiochim. Acta*, 2020, **108**, 727–735.
54 Y. L. Hou, Y. Diao, Q. Jia and L. Chen, *ACS Omega*, 2020, **5**, 7392–7398.
55 Z. Shiri-yekta, M. R. Yaftian and A. Nilchi, *Korean J. Chem. Eng.*, 2013, **30**, 1644–1651.
56 C. Zhao, P. Gu, X. Liu, T. Wen and Y. Ai, *Environ. Sci.: Water Res. Technol.*, 2020, **6**, 1482–1494.